Bulletin of Mathematical Biology (2006) 68: 1039–1051
DOI 10.1007/s11538-006-9113-9

ORIGINAL ARTICLE

From Biochemistry to Morphogenesis in Myxobacteria

Oleksii Sliusarenko, Jing Chen, George Oster*

University of California, Berkeley, CA, USA

Received: 30 September 2005 / Accepted: 17 February 2006 / Published online: 20 June 2006

Abstract Many aspects of metazoan morphogenesis find parallels in the communal behavior of microorganisms. The cellular slime mold *D. discoideum* has long provided a metaphor for multicellular embryogenesis. However, the spatial patterns in *D.d.* colonies are generated by an intercellular communication system based on diffusible morphogens, whereas the interactions between embryonic cells are more often mediated by direct cell contact. For this reason, the myxobacteria have emerged as a contending system in which to study spatial pattern formation, for their colony strutures rival those of *D.d.* in complexity, yet communication between cells in a colony is carried out by direct cell contacts. Here I sketch some of the progress my laboratory has made in modeling the life cycle of these organisms.

Keywords Bacterial locomotion · Gliding motility · Morphogenesis · Myxobacteria · Myxococcus · Pattern formation

1. Introduction: Myxobacteria mysteries

In 1971, as a postdoc, I attended my first Theoretical Biology Gordon Research Conference, chaired that year by Simon Levin. There Simon introduced me to Lee Segel, and my life changed. Although we talked science innumerable times, I never coauthored a paper with Lee. However, he has been one of the intellectual *spiritus movens* in my scientific career. Moreover, he introduced me to two of my most significant collaborators: Garry Odell and Jim Murray. Lee always saw further and deeper than the rest of us, and frequently pointed us in directions we might not have otherwise traveled. As luck would have it, I was able to contribute a small bit back to Lee, for some of his work in theoretical immunology using a tool that I had introduced with Alan Perelson in 1979, so-called "shape space," whose implications I did not discern at the time. Because of Lee's early work with Evelyn Keller on pattern formation in *E. coli*, and through my collaborations with Garry and Jim, my research returned periodically to the mysteries of morphogenesis,

* Corresponding author.
E-mail address: goster@nature.berkeley.edu (G. Oster).

although in a number of different settings. Most recently, this recurrent theme arose once again, this time in the setting of bacterial pattern formation.

Myxococcus xanthus is a humble organism; it causes no diseases, but lives obscurely on the forest floor where it glides slowly in large assemblies over surfaces in search of its prey. The story of these organisms might have remained in obscurity but for the research of Dale Kaiser, whose laboratory at Stanford has devoted several decades to unraveling the many mysteries of their amazingly complex life cycle. A chance encounter with Dale at a meeting ignited my curiosity and led to a number of investigations that shed some light on the mechanisms underlying the mysteries. Here I will sketch some recent explorations in my laboratory.

At the time I met Dale, I was struck by three aspects of myxobacteria morphogenesis. First, was the puzzle of how they moved. Bacteria move in many more ways than eukaryotic cells; swimming bacteria can propel themselves using rotary propellers, or flagella. Some, like marine cyanobacterium *Synechococcus* swim with no detectable surface organelles; how they accomplish this remains mysterious (McCarren et al., 2005). Other bacteria move smoothly across surfaces, a means of locomotion called 'gliding'. In most cases, no one knows how they do this. However, in myxobacteria, some things have come to light recently (Kaiser, 2004; Kaiser and Welch, 2004; Nudleman and Kaiser, 2004; Nudleman et al., 2005). These bacteria have two ways of moving, called A (adventurous) and S (social) motility (McBride, 2000, 2001). As the name suggests, the former works for isolated bacteria, and the latter works only when they move in groups.

A-motility is associated with slime secretion, and individuals tend to follow slime trails laid down by recent passersby. Recently, we were able to show that the thrust generated by the polyelectrolyte slime emerging from nozzles at the cell poles could account for the observed speed of S^- mutants (Wolgemuth et al., 2002). S-motility is accomplished by the extension, attachment, and retraction of type 4 pili (Nudleman and Kaiser, 2004). Retraction is driven by a hexameric motor called PilT, which can generate $\sim$120 pN of force, the strongest of any known protein motor (Maier et al., 2002, 2004).

Under normal conditions, both motors operate in tandem: the pili extending from the anterior pole, pulling the cell forwards, and the slime extruding from the posterior nozzles, pushing the cell in the same direction. A cell reverses its direction of gliding not by turning, but by switching the polarity of its motors: the pili retract from one end and commence extending from the other, while the slime extrusion also switches ends. It is not known how this switch is carried out, but recently it was found that the switch is foretold by the fast migration of a motility protein (FrzS) from the anterior to posterior pole (Mignot et al., 2005).

As individuals, myxobacteria behave in a very boring way. They simply oscillate back and forth, reversing direction every few minutes. Moreover, they move quite slowly, less than one body length (4–6 μm) per min. But myxobacteria are social organisms whose life depends on moving in very large groups. This is because, despite their leisurely speed, they are predators. Their prey include swimming bacteria like *E. coli* that move hundreds of times faster than they glide. They accomplish this by secreting peptides and exoenzymes that attract other bacteria and then digest them externally, allowing the myxobacteria to absorb their amino acids from the deadly soup surrounding the colony. An individual bacterium could not secrete

sufficient amount of enzymes to incapacitate a prey, and so remaining within the "wolf pack" of swarming compatriots is essential. Thus the oscillations of isolated individuals is a good strategy, increasing the probability of being reabsorbed by the streaming colony rather than wandering off randomly.

The swirling and swarming of a myxobacteria colony can be followed in time-lapse cinematography; but their really interesting behavior does not manifest itself until food runs scarce, and the cells commence to revert to starvation mode. To survive the famine, cells begin to stream into large aggregations, or "fruiting bodies" where they sporulate and lie dormant until better times reappear (Kaiser, 2004; Kaiser and Welch, 2004; Kaiser and Yu, 2004). Figure 1 shows a sequence of snapshots of the life cycle.

In laboratory cultures, colonies on their way to fruiting body formation generate elaborate wave patterns that are unlike any other observed in biology, chemistry, or physics (Igoshin et al., 2004c, 2001; Sager and Kaiser, 1994; Welch and Kaiser, 2001). Figure 2a shows an example of these waves. While the fruiting bodies in laboratory strains of *M. xanthus* are simple mounds of cells and spores, related species of myxobacteria produce much more elaborate structures, with symmetrical arms reminiscent of slime mold fruiting bodies. Figure 2b shows one example. A combination of theoretical and experimental investigations has begun to unravel the mysteries of myxobacteria morphogenesis. Here we will sketch a sampling of these investigations.

2. Accordion waves

One of the most striking phenomena associated with myxobacteria morphogenesis is their collective developmental waves. This 'ripple phase' appears before or during the formation of fruiting bodies (Igoshin et al., 2001, 2004b; Welch and Kaiser, 2001; Kaiser and Welch, 2004; Sliusarenko et al., 2006). These waves may be a delicate phenomenon, since they have not yet been observed outside laboratory cultures. However, despite their lack of "robustness"—indeed, *because* of it—they provide the key to understanding the later stages of colony morphogenesis for they reflect key properties of the intercellular communication system.

Two kinds of laboratory cultures have been developed to study the ripple phase, the submerged culture of Roy Welch in Dale Kaiser's lab (Welch and Kaiser, 2001), and the monolayer culture of Oleksii Sliusarenko in David Zusman's lab (Sliusarenko et al., 2006). Each reveals important aspects of the ripple phase. Figure 3a shows density waves swirling around the periphery of a multilayer submerged culture. Movies of the waves can be retrieved from Sliusarenko et al. (2006). They show a striking phenomenon: when the waves collide, they appear to pass through one another unaffected, analogous to soliton waves in fluids. But this is an illusion. Closer inspection reveals that the waves actually reflect off one another. Further, following fluorescently marked individuals shows that every cell is simply oscillating back and forth; only the cell density gives the appearance of propagating waves. We call this illusion "*accordion waves*" to distinguish them from the more familiar waves generated by *D. discoideum* colonies where

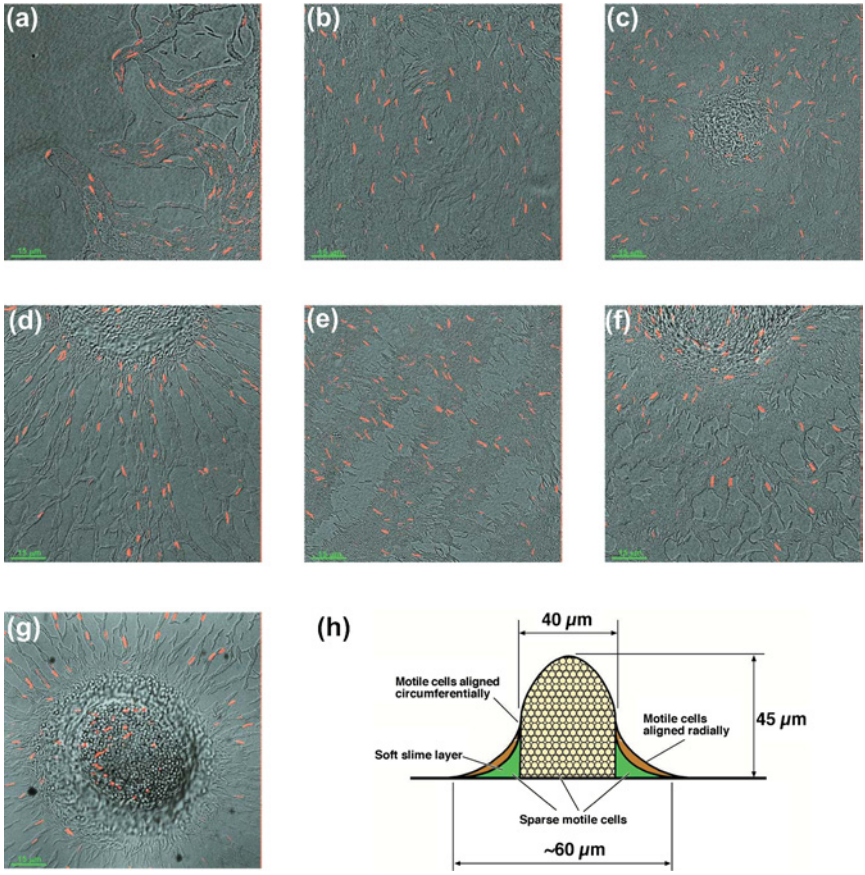

Fig. 1 Stages of myxobacterial development taken from the movies. Individual cells in a monolayer culture can be florescently tagged (*red* in these photos) and followed. (a) swarming stage (high nutrients). (b) After 8 h of starvation, in the interior of the colony almost no structure is visible. (c) After 10 h of starvation, aggregate formation has started. (d) After 24 h of starvation ripples commence, along with streams (e), (f) Ripples around a young fruiting body. (h) After 48 h of starvation the mature fruiting body with spores has formed (h) A schematic cross-section of a fruiting body.

colliding waves annihilate one another, similar to waves in diffusion-reaction systems.

The monolayer culture provides a close-up view of what happens when waves collide. Figure 3b,c shows two wavefronts colliding. Movies of these monolayer collisions reveal much about the mechanism that generates the accordion waves. In particular, they arise from the synchronized behavior of many cells, each of which is oscillating back and forth in place. To model this process we first discuss the basis of individual oscillations.

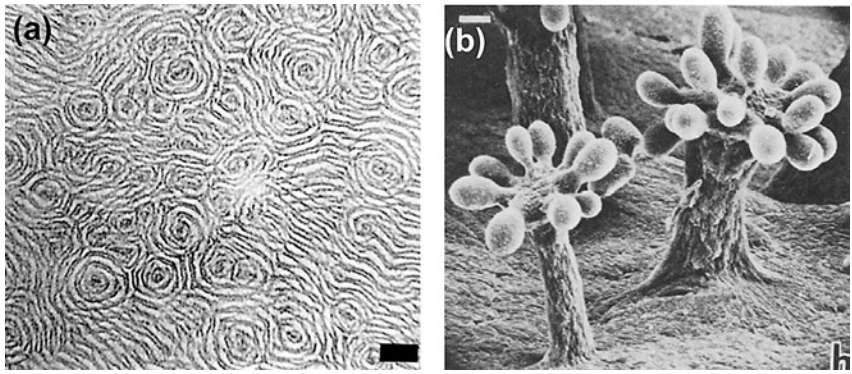

Fig. 2 Myxobacteria morphogenesis. (a) Ripple phase showing concentric, spiral, and parallel waves (from Sager and Kaiser, 1994). (b) Fruiting bodies of a related myxobacteria species *C. crocatus* (from Grilione and Pangborn, 1975).

3. The Frizilator

Understanding the collective behavior of myxobacteria begins with the behavior of isolated individuals. When separated from its hunting colony swarm a bacterium will simply oscillate back and forth, with no net drift in any direction. These reversals are not random; that is, the residence times in the "forward" and "reverse" directions are not exponentially distributed. This suggests strongly that reversals are controlled by an internal biochemical oscillator, the "reversal clock" (Igoshin et al., 2004a). However, the clock is not very precise; the oscillation period is about 8 min, but with a variance of 3–4 min. A substantial body of experiments, both biochemical and genetic, has elucidated a great deal of the circuitry that controls the reversals; this is summarized in Fig. 4a. The essence of the circuit is a chain of three covalent modifications of proteins in the *frz* gene system (Bustamante et al., 2004). A feedback is required to turn this highly nonlinear system into an oscillator. Several pathways will work, and the one shown in the figure is the most likely prospect, and the one we have incorporated into the model.

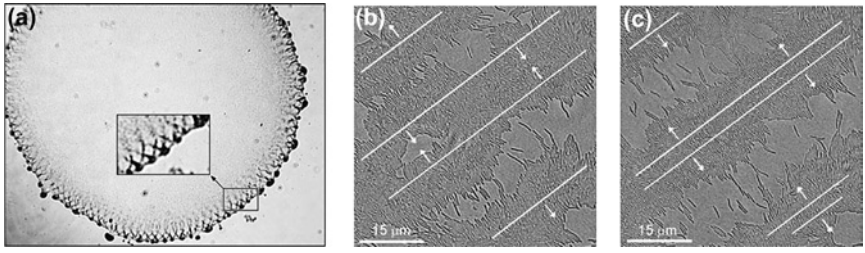

Fig. 3 Ripple phase cultures. (a) Waves around the periphery of a submerged multilayer culture (from Welch and Kaiser, 2001). The inset is a closeup of the waves showing the fruiting bodies forming at loci where the waves intersect. (b) Closeup of waves in a monolayer culture (from Sliusarenko et al., 2006).

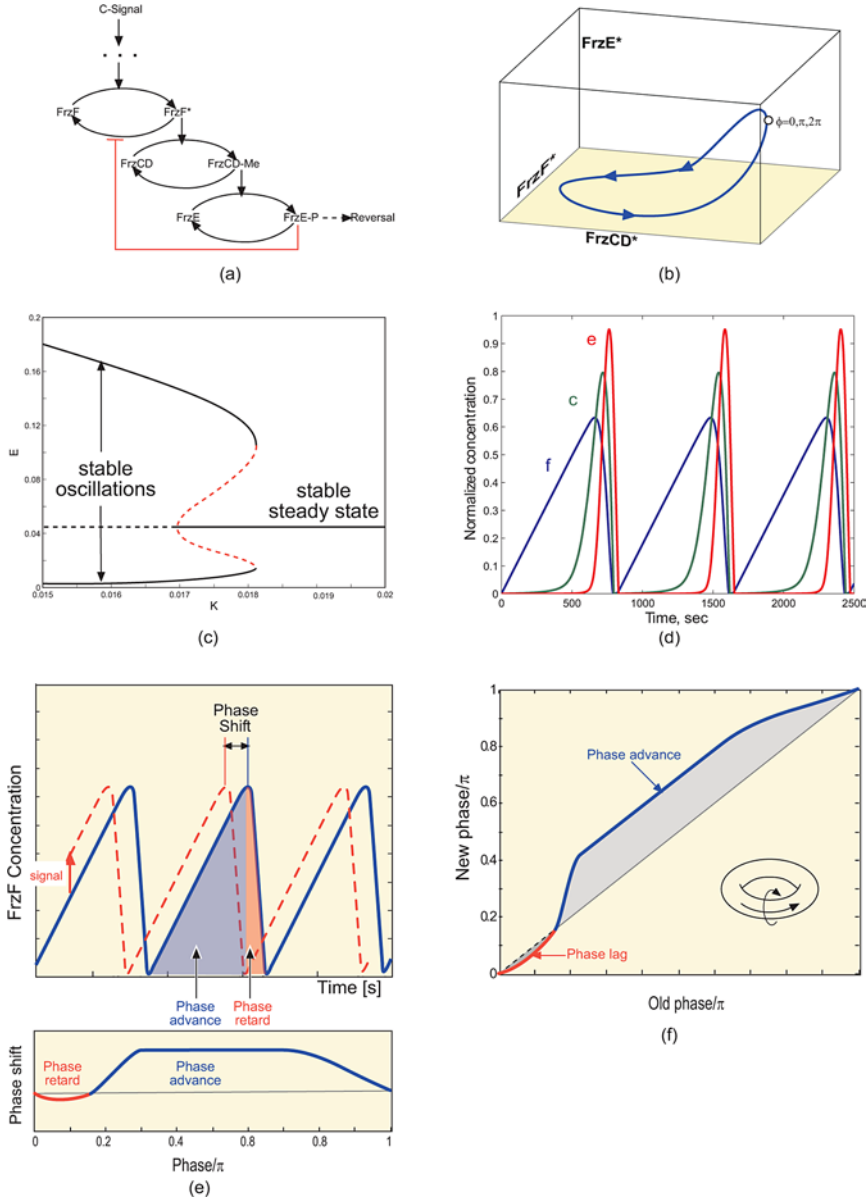

Fig. 4 The Frizilator model. (a) Schematic represtation of the Frizilator oscillator based on a chain of phosphorylation-methylation-phosphorylation modifications with a negative feedback. (b) Representation of the limit cycle in the concentration space. (c) Bifurcation diagram of [FrzE] oscillation amplitude vs. Michaelis–Menten saturation concentration showing the subcritical bifurcation. The *solid* and *dashed lines* show the stable and unstable regions, respectively. (d) The concentration waveforms of the active enzymes plotted vs. time. (e) The phase shift effect on the oscillation due to an impulse signal in the concentration of FrzF. (f) The resetting map of the frizilator: the new phase of the clock after receiving the same signal at different initial phase points.

For notational convenience, we neglect the "Frz" in the proteins' names. We consider that each covalent modification obeys Michaelis–Menten kinetics. Then the variables can be expressed in terms of the activated fraction of each protein, defined as

$$\begin{aligned} f &= \frac{[F^*]}{[F^*]+[F]}, \\ c &= \frac{[\mathrm{CD}^*]}{[\mathrm{CD}^*]+[\mathrm{CD}]}, \\ e &= \frac{[E^*]}{[E^*]+[E]}, \end{aligned} \tag{1}$$

where the letters with a star are the activated forms and without star the inactive forms. Then the dynamics of the system is governed by:

$$\begin{aligned} \frac{\mathrm{d}}{\mathrm{d}t} f &= \frac{V_a(1-f)}{K_a+(1-f)} - e\,\frac{V_d\, f}{K_d+f}, \\ \frac{\mathrm{d}}{\mathrm{d}t} c &= f\,\frac{V_m(1-c)}{K_m+(1-c)} - \frac{V_{\mathrm{dm}}c}{K_{\mathrm{dm}}+c}, \\ \frac{\mathrm{d}}{\mathrm{d}t} e &= c\,\frac{V_p(1-e)}{K_p+(1-e)} - \frac{V_{\mathrm{dp}}e}{K_{\mathrm{dp}}+e}. \end{aligned} \tag{2}$$

When the parameters taken from experiments are inserted into Eq. (2), they generate a limit cycle like that shown in Fig. 4b. The waveforms of *f, c*, and *e* are shown in Fig. 4d: $f(t)$ is a sawtooth, and $e(t)$ is nearly a spike train. Cell reversals are triggered by the spikes in *e*. When this limit cycle is installed into the agent model described below, we will see that the spatial patterns are affected by several features of these oscillations.

1. Individual cells oscillate in place, or remain stationary. While the amplitude of the oscillations is variable, their onset is all-or-none: i.e., not as smoothly increasing amplitude. This is consistent with the finding shown in Fig. 4c: the onset of oscillations in the Frizilator takes place via a subcritical Hopf bifurcation.
2. The waveform of the signal receiving component, FrzF ($f(t)$ in Eq. (2)), is asymmetrical, as shown in Fig. 4d. Thus a random perturbation in the cycle is much more likely to hit the rising portion of the FrzF oscillation than the falling portion.
3. The limit cycle is fairly 'stiff'. That is, a perturbation of the cycle by an impulse in FrzF returns the system to its limit cycle quickly, within one period.

Property 3 will permit us to replace the limit cycle by a phase-resetting map in the mean field model. This is shown schematically in Fig. 4e. A collision induced perturbation in FrzF results in a nearly immediate shift in the phase, $\phi(t)$, of the

oscillations by an amount $\Delta\phi$. The phase magnitude of the phase shift as a function of the phase of the perturbation is shown in the bottom part of Fig. 4e. The asymmetry of the waveform in $f(t)$ is reflected in the asymmetry of the resetting map: phase advances are much more likely than phase retardations because the duration of the increasing part of the $f(t)$ sawtooth is much longer than the decreasing part. Figure 4f shows a common representation of the signaling event as a phase resetting map of new phase vs. old phase. Both old and new phases are periodic, so that the phase on top (right) and the phase resetting map is identical to the phase on the bottom (left) (Winfree, 2001; Oster, 2004). Thus the phase resetting process can be viewed as a flow on a torus (inset in Fig. 4f).

Finally, the limit cycle specified by Eq. (2) specifies a fixed period of oscillation, which is surely not realistic. The simplest remedy is to add random terms, $r_i(t)$, to each equation to simulate the effect of diffusion in the phase.

4. Driving morphogenesis with the Frizilator

The most straightforward way to model a population of motile cells is to construct an "agent" model that tracks the position and orientation of each cell. Such models have been used in a variety of settings (Schweitzer, 2003). Their advantage is that they are easy to program and one can incorporate elaborate rules of "behavior." Their disadvantage compared to mean field models is that it is frequently difficult to intuit global insights from simulations alone. Therefore, we attacked the problem from both perspectives.

4.1. Agent model

We track a single bacterium by writing Newton's second law with an added force generated by the bacterial motor, $\mathbf{F}_{\mathrm{m}}$: $m\,\mathrm{d}\mathbf{v}/\mathrm{d}t = -\zeta\mathbf{v} + \mathbf{F}_{\mathrm{m}} + r(t)$, where m is the bacterial mass, ζ is the drag coefficient between the bacterium and the slime, and $r(t)$ is a random force. To write this in components, we use the coordinates shown in Fig. 5a to track individual bacteria. The position of the cell center is given by

$$\text{Position}: \quad \frac{\mathrm{d}}{\mathrm{d}t}x = v\,\cos(\theta), \quad \frac{\mathrm{d}}{\mathrm{d}t}y = v\,\sin(\theta), \tag{3}$$

where the cell orientation, $\theta(t)$, with respect to the horizontal is computed from

$$\text{Orientation}: \quad \frac{\mathrm{d}}{\mathrm{d}t}\theta = \underbrace{-\sum_{j:|\vec{r}_j-\vec{r}_i|\le r_0}\frac{\sin(2(\theta_i-\theta_j))}{\tau_\theta}}_{\text{Alignment with neighbors}} + \underbrace{\pi\,\delta(t-t_{\mathrm{rev}})}_{\text{Collision induced reversal}} + \underbrace{r_\theta(t)}_{\text{Angular fluctuations}} \tag{4}$$

In the first term on the right-hand side the summation is over all neighbor cells, j, the centers of which are separated by no more than a constant, r_0, from the test

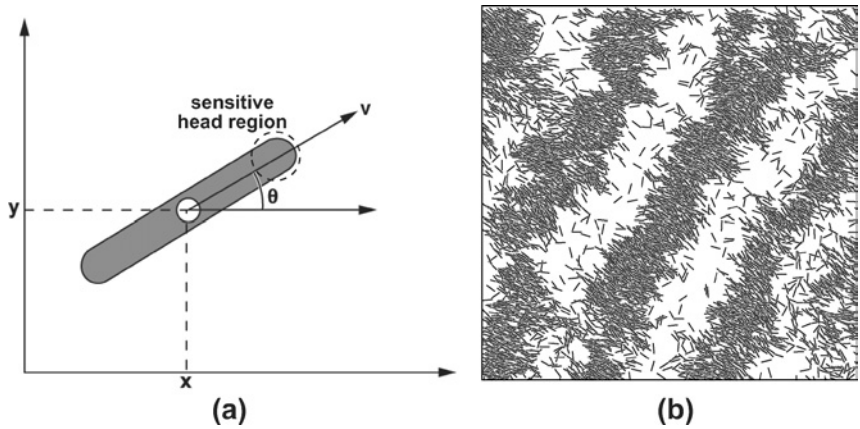

Fig. 5 Agent model. (a) Coordinate representation of one cell. A cell is characterized by its coordinates **x** and **y**, its orientation θ and its speed **v**. Two counter-aligned cells interact when their head regions overlap. (b) A snapshot of the simulations showing the wave pattern at the moment of wave collision.

cell, *i*. θ_j and θ_i are the orientation angles of these cells. This term accounts for the steric tendency of the rod shaped cells to align with one another (see Appendix A of Csahok and Czirok (1997) for the derivation). Autonomous reversals due to the cellular reversal clock are accounted for by installing the Frizilator limit cycle into each cell. The second term in (4) with the Dirac delta function represents the reversals of the cells when the orientation rapidly changes by π. Randomness in phase is accounted for by random terms in the Frizilator Eq. (2). The speed of the cells is maintained nearly constant by imposing a relaxation time, $\tau = m/\zeta$ that returns the speed to its average value, $v_0 = \mathbf{F}_m/\zeta$ determined by the force balance between the propulsion motors and the frictional drag:

$$\text{Speed}: \quad \frac{\mathrm{d}}{\mathrm{d}t}v = \underbrace{-\frac{(v - v_0)}{\tau_v}}_{\text{Relaxation of speed to } v_0} + \underbrace{r_v(t)}_{\text{Fluctuations in speed}} . \tag{5}$$

In order to accurately model the accordion waves, one final ingredient is necessary. Cell-to-cell signaling must by *asymmetric*: head-to-head collisions are much more effective mediators of cell signaling than head-to-tail collisions. The rationale for this is that S-motility pili can pull head-to-head colliding cells into outer membrane contact where receptor–ligand signaling can take place (Nudleman et al., 2005). However, head-to-tail collisions encounter the resistance of the viscoelastic slime extruded from each cell's posterior (Wolgemuth et al., 2002); this is sufficient to make cell contact much less likely. A few possible mechanisms to determine the moment of collision can be implemented numerically. The rule for collisions used in these simulations considered two cells interacting if their leading edges were located within a certain interaction distance (∼one cell diameter), and the signaling

strength was maximum for opposite moving cells and zero for aligned cells; i.e.:

$$S \propto \sin\left[(\theta_i - \theta_j)/2\right]^2 .$$

Installing the Frizilator limit cycle into each cell, simulations of the model Eqs. (1)–(5) were carried out for $\sim 10^5$ cells. A frame from the movie is shown in Fig. 5b. The model reproduces the monolayer experiments rather closely, except for certain effects that depend on the finite size of cells (see Sliusarenko et al., 2006).

4.2. Mean field model

While it is satisfying that the agent model can reproduce the accordion waves, additional insight into their character can be gleaned from an approximate mean field model that tracks only the local cell density. This approach was quite successful in modeling the multilayer cultures (Igoshin et al., 2001, 2004a,b,c,d; Igoshin and Oster, 2003). However, in the monolayer cultures the area cell density is usually either near zero or unity, and so the mean field approach is less valid. The model described here is based on the paper by Igoshin et al. (2001) with modifications to make it compatible with the agent-based model described above. The major modification is removing the unnecessary assumption of nonlinear density dependence in intercellular signaling.

For simplicity, we describe only the situation corresponding to the multilayer waves (containing more cells) shown in Fig. 3a where cells are moving mostly parallel to the x-axis (parallel to the edge of the colony). Then we can write a conservation equation for the cell density in space and phase, $n(t, x, y, \phi)$:

$$\frac{\partial n_\pm}{\partial t} = \underbrace{-\left[\frac{\partial n_\pm}{\partial x} + \frac{\partial}{\partial \phi}\left(\omega_\pm n_\pm\right)\right]}_{\text{Convection in space and phase}} + \underbrace{\left[D_x \frac{\partial^2 n_\pm}{\partial x^2} + D_y \frac{\partial^2 n_\pm}{\partial y^2} + K \frac{\partial^2 n_\pm}{\partial \phi^2}\right]}_{\text{Diffusion in space and phase}}, \quad 0 < \phi < \pi,\ t > 0 \tag{6}$$

Here the $(\pm)$ subscript refers to cells moving to the right and left; i.e., counterclockwise or clockwise along the colony periphery. $D_{x,y}$ are the spatial diffusion coefficients and K is the phase diffusion coefficient. The boundary conditions were chosen periodic.

This must be augmented by the phase resetting map that specifies what happens—on average—when opposite-moving cells collide. Thus the phase velocity, $\omega_\pm$, can be tracked via the resetting map, $\psi(\phi)$, as discussed above:

$$\omega_\pm = \underbrace{\omega_0}_{\text{Unperturbed phase velocity}} + \overbrace{\underbrace{\omega_1}_{\text{Amplitude}}\ N_\mp(x, y, t)\ \underbrace{\psi(\phi)}_{\text{Resetting map}}}^{\text{Collision induced phase resetting}}, \tag{7}$$

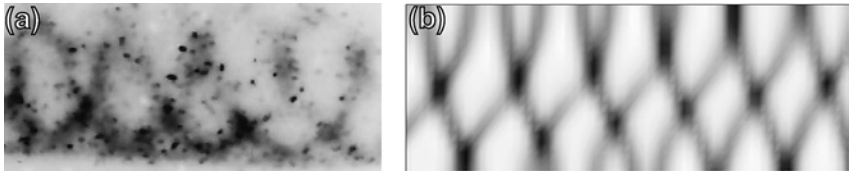

Fig. 6 Experimental (a) and mean field model of the peripheral waves in Fig. 3a. In the model, the tilt is a consequence of the curvature of the colony edge.

where $N_{\pm} = \int_0^{\pi} n_{\pm}(t, x, y, \phi)\, \mathrm{d}\phi$ is the density of opposite-moving cells.

Figure 6a and b shows that the mean field model predicts well the peripheral waves in the multilayer colony of Fig. 3a. Moreover, the wavelength, λ, predicted by the mean field model is

$$\lambda \approx 2 \langle v \rangle T_{\mathrm{rev}} \tag{8}$$

where $\langle v \rangle$ is the mean gliding velocity and T_{rev} is the mean time between reversals. It turns out that the spacing of the fruiting bodies around the periphery of the submerged colony in Fig. 3a is approximately equal to the wavelength. Cells can be observed streaming between adjacent fruiting bodies, with larger aggregations growing at the expense of smaller ones until the final spacing is achieved. This can be understood by realizing that individual bacteria, since they signal by direct contact only, have no information about cell density further away than the distance they can glide before reversing. This is their "event horizon," to borrow a term from astrophysics (see Fig. 7a). Moreover, the larger the aggregation of a forming fruiting body, the longer will the residence time of a bacterium in it before escaping to stream to an adjacent aggregation. Thus larger aggregations will grow and smaller ones will shrink.

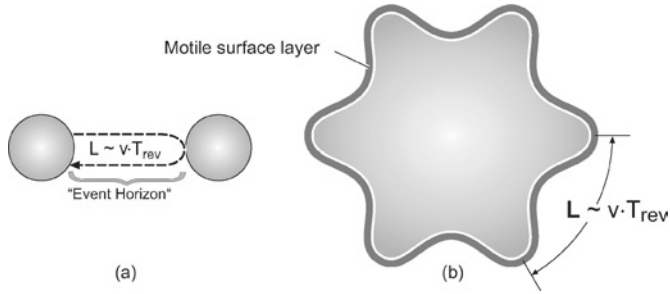

Fig. 7 The morphogenetic length scale. (a) The spacing of fruiting bodies along the periphery of a colony in the multilayer culture is determined by the "event horizon": each cell senses cell density only one reversal distance away (Welch and Kaiser, 2001). (b) Spacing of protrusions on a branching fruiting body presumably follows the same rule.

5. Conclusion: A long journey begun

Our modeling studies demonstrate that the existence of the accordion waves require several ingredients. First, each cell contains an internal biochemical oscillator whose waveform is asymmetric, so that phase advances are more likely than phase retardations. Second, cell signaling is via direct cell contact and is asymmetric, so that head-to-head collisions shift the clock phase more than head-to-tail collisions.

The agent and mean field models complement one another. For example, the agent model shows the effects of the limit cycle properties on the patterns, and the mean field model gives an estimate of the wavelength. Together, they give confidence that we understand the basic principles underlying these unique morphogenetic patterns. But what about the later stages of morphogenesis? A key observation gives hope that the models will have something to say about the growth of elaborate structures such as those shown in Fig. 2b. The monolayer cultures frequently give way to multilayer swarms, where several tiers of cells glide more or less independently on top of one another, like floors in a parking structure. They are actually gliding on slime layers that separate the tiers, and so their directions are only loosely correlated. This layered quality persists into the formation of the fruiting body.

The last panel in Fig. 1 shows a cross section of a fruiting body deduced from a movie where the focal plane was moved vertically to obtain a "cat-scan" of the fruiting body structure. The experiments revealed that the fruiting body is a layered structure wherein the volume fraction of the cells is not more than 50%, the rest being hydrated slime. In the center of the fruiting body are spores, and cell migration is mainly on the surface layer or two. Consequently, the same length scale set by the "event horizon" in Eq. (8) constrains the spacing of the surface aggregations that will grow into the "arms" shown in Fig. 2b. This is shown schematically in Fig. 7b.[1] Thus, the hope is that the pattern scale deduced from the ripple phenomenon will repeat itself at higher levels of organization. And perhaps the insights gained from this humble bacterium may provide clues to pattern formation in higher organisms. For example, the formation of somites in vertebrates, that arises from cellular clocks synchronized by direct contact in a wave-like fashion (Holley and Takeda, 2002; Lewis, 2003).

References

Bustamante, V., Martinez-Flores, I., Vlamakis, H., Zusman, D., 2004. Mol. Microbiol. 53, 1501–1513.
Csahok, Z., Czirok, A., 1997. Physica A: Stat. Theor. Phys. 243, 304–318.
Grilione, P., Pangborn, J., 1975. JB 124, 1558–1565.
Holley, S.A., Takeda, H., 2002. Semin. Cell Dev. Biol. 13, 481–488.
Igoshin, I., Goldbeter, A., Kaiser, A.D., Oster, G., 2004a. PNAS 101(44), 15760–15765.

[1] By constrast, the length scale that sets the patterns in systems governed by diffusion/reaction equations arises from a Turing instability that depends on ratios of diffusion coefficients. In the myxo models, the length scale arises in a very different way from the convective term in the equation of motion.

Igoshin, I., Oster, G., 2003. Math. Biosci. 188, 221–233.
Igoshin, I., Welch, R., Kaiser, D., Oster, G., 2004b. PNAS 101, 4256–4261.
Igoshin, O., Kaiser, D., Oster, G., 2004c. Curr. Biol. 14, R459–R462.
Igoshin, O., Mogilner, A., Welch, R., Kaiser, D., Oster, G., 2001. PNAS 98, 14913–14918.
Igoshin, O., Neu, J., Oster, G., 2004d. Phys. Rev. E 70, 1–11.
Kaiser, D., 2004. Ann. Rev. Microbiol. 58, 75–98.
Kaiser, D., Welch, R., 2004. J. Bacteriol. 186, 919–927.
Kaiser, D., Yu, R., 2004. Department of Developmental Biology, Stanford University, pp. 1–10.
Lewis, J., 2003. Curr. Biol. 13, 1398–1408.
Maier, B., Koomey, M., Sheetz, M., 2004. PNAS 101, 10961–10966.
Maier, B., Potter, L., So, M., Seifert, H., Sheetz, M., 2002. PNAS 99, 16012–16017.
McBride, M., 2000. Am. Soc. Microbiol. News 66, 203–210.
McBride, M., 2001. Am. Rev. Microbiol. 55, 49–75.
McCarren, J., Heuser, J., Roth, R., Yamada, N., Martone, M., Brahamsha, B., 2005. J. Bacteriol. 187, 224–230.
Mignot, T., Merlie, J., Zusman, D., 2005. Science 310(5749), 855–857.
Nudleman, E., Kaiser, D., 2004. J. Mol. Microbiol. Biotechnol. 7, 52–62.
Nudleman, E., Wall, D., Kaiser, D., 2005. Science 309, 125–127.
Oster, G., 2004. J. Theor. Biol. 230, 451–458.
Sager, B., Kaiser, D., 1994. Genes Dev. 8, 2793–2804.
Schweitzer, F., 2003. Brownian Agents and Active Particles: Collective Dynamics in the Natural and Social Sciences. Springer-Verlag, Berlin.
Sliusarenko, O., Zusman, D., Oster, G., 2006. PNAS 103(5), 1534–1539.
Welch, R., Kaiser, D., 2001. PNAS 98, 14906–14912.
Winfree, A., 2001. The Geometry of Biological Time. Springer-Verlag, Berlin, New York.
Wolgemuth, C., Hoiczyk, E., Kaiser, D., Oster, G., 2002. Curr. Biol. 12, 369–377.